

Hyperuniformity near jamming transition over a wide range of bidispersity

Duc T. Dam,^{1,*} Takeshi Kawasaki,^{1,2} Atsushi Ikeda,³ and Kunimasa Miyazaki^{1,†}

¹*Department of Physics, Nagoya University, 464-8602 Nagoya, Japan*

²*D3 Center, Department of Physics, Osaka University, Toyonaka, Osaka 560-0043, Japan*

³*Graduate School of Arts and Sciences, The University of Tokyo, Tokyo 153-8902, Japan*

(Dated: July 18, 2025)

We numerically investigate hyperuniformity in two-dimensional frictionless jammed packings of bidisperse systems. Hyperuniformity is characterized by the suppression of density fluctuations at large length scales, and the structure factor asymptotically vanishes in the small-wavenumber limit as $S(q) \propto q^\alpha$, where $\alpha > 0$. It is well known that jammed configurations exhibit hyperuniformity over a wide range of wavenumbers windows, down to $q^* \sigma \approx 0.2$, where σ is the particle diameter. In two dimensions, we find that the exponent α is approximately 0.6–0.7. This contrasts with the reported value of $\alpha = 1$ for three-dimensional systems. We employ an advanced method recently introduced by Rissone *et al.* [Phys. Rev. Lett. **127**, 038001 (2021)], originally developed for monodisperse and three-dimensional systems, to determine α with high precision. This exponent is found to be unchanged for all size ratios between small and large particles, except in the monodisperse case, where the system crystallizes.

I. INTRODUCTION

Hyperuniform systems are a distinct state of matter in which density fluctuations are anomalously suppressed at large length scales [1, 2]. For equilibrium systems in d dimensions, the particle number fluctuation $\langle \delta N^2 \rangle = \langle N^2 \rangle - \langle N \rangle^2$ within a subsystem of size R is extensive, *i.e.*, $\langle \delta N^2 \rangle \propto \langle N \rangle \propto R^d$. Equivalently, in Fourier space, the static structure factor $S(q) = \frac{1}{N} \langle |\delta \rho(\mathbf{q})|^2 \rangle$, where $\delta \rho(\mathbf{q})$ is the density fluctuation at wavenumber \mathbf{q} , remains constant in the large-scale limit $q \equiv |\mathbf{q}| \rightarrow 0$. In contrast, for hyperuniform systems, $\langle \delta N^2 \rangle$ becomes sub-extensive and scales in the large- R limit as $R^{d-\alpha}$, while $S(q)$ vanishes in the small- q limit as

$$S(q) \propto q^\alpha \quad \text{for } q \rightarrow 0, \quad (1)$$

where $\alpha > 0$ is a positive *hyperuniformity exponent* that characterizes the degree of hyperuniformity.

Over the past few decades, hyperuniformity has been identified in a variety of nonequilibrium systems, including fluctuations in the early universe [3], avian photoreceptor patterns [4], receptor organization in the immune system [5], and glasses [6]. The packing of frictionless spheres near the jamming transition is among the earliest known examples of hyperuniform systems [1, 7–10].

The jamming transition occurs when athermal soft particles cease flowing and the system acquires rigidity, forming an amorphous solid as the packing fraction φ increases beyond a critical value φ_J [11–13]. The jamming transition of frictionless particles is characterized by several critical behaviors [12, 13]. Examples include the algebraic dependence of various quantities, such as the contact number δz and shear modulus G , on the dis-

tance to jamming $\delta \varphi = \varphi - \varphi_J$, as well as the emergence of diverging collective length scales and universal low-frequency vibrational modes. Although these critical behaviors have been well explained by geometric variational arguments [14] and mean-field theory [15], the hyperuniform behavior of jammed systems remains outside the scope of these arguments, and the connection between the jamming transition and hyperuniformity is poorly understood.

Hyperuniformity in jammed packings was first reported in Ref. [1], which showed that $S(q) \propto q$ (*i.e.*, $\alpha = 1$). This behavior has since been investigated further in numerous studies [7, 16–22]. Torquato and Stillinger conjectured that any strictly jammed, saturated, infinite packing of monodisperse spheres in d dimensions is hyperuniform with $\alpha = 1$, provided that the configuration is “maximally disordered” [1, 2, 23].

A closer inspection of $S(q)$ at small wavenumbers reveals that the algebraic hyperuniform behavior persists only down to a finite q . As q decreases further, $S(q)$ either saturates [16, 22, 24] or even increases in systems with broad particle size distributions [16, 25]. This departure from hyperuniformity was attributed to density fluctuations of different components in size-disperse systems [16]. Such binary or multicomponent mixtures are commonly used to avoid crystallization when generating disordered jammed states. In order to mitigate the undesirable fluctuations arising from different components and size disparity, several variants of $S(q)$ have been proposed and studied. Examples include the q -dependent isothermal compressibility $\chi_T(q)$ defined by a spectrum of the linearly combined densities of different components [16], the spectral density $\chi(q)$ defined in terms of the fluctuations that weight particles by their area [16, 17], and the local volume fraction fluctuation $\chi_V(q)$ [8, 9, 17]. These revised observables successfully reduce the fluctuations of the concentrations, yet they consistently show clear hyperuniform behavior only at $q > q^* \approx 0.2/\sigma_{\text{ave}}$, where σ_{ave} is an average particle

* dam@r.phys.nagoya-u.ac.jp

† miyazaki@r.phys.nagoya-u.ac.jp

diameter. Although the fate of hyperuniformity at the smaller wavenumber limit remains elusive, previous studies have unanimously claimed $\alpha = 1$ in the intermediate regime $q > q^*$ for jammed packings generated using standard protocols both in two [16–20] and three dimensions [1, 7, 16, 21, 22].

Recently, we investigated density fluctuations in two-dimensional mixtures near φ_J and reported a smaller hyperuniformity exponent, $\alpha \approx 0.7$ [26]. This value has proven robust and insensitive to the different annealing protocols used to prepare the packings. The deviation from previously reported exponents in three-dimensional systems is somewhat surprising, given that the upper critical dimension of the jamming transition is $d_c = 2$. In this study, we re-examine the hyperuniformity exponent for two-dimensional packings with high accuracy. We use a standard protocol to generate jammed packings: slow isotropic compression toward the jamming transition density φ_J . In the previous study, we investigated only an equimolar bidisperse system with a size ratio of 1:1.4 between small and large particles, an archetypal and widely used model system in studies of the jamming transition. Here, we extend the analysis across a wide range of size ratios, $f_r = \sigma_S/\sigma_L$, from 0.3 to the monodisperse limit of 1. The particle size distribution significantly affects the jamming transition density φ_J and local structural features [27–29], whereas critical scaling properties remain insensitive to size disparity [28, 30–32]. Notably, recent studies have shown that jamming criticality persists near φ_J even as the size ratio approaches unity and the system becomes increasingly crystalline. However, the range over which critical scaling is observed narrows progressively in the monodisperse limit, $f_r \rightarrow 1^-$ [33, 34]. The point $f_r = 1$ is singular, as the system forms an ideal crystal and exhibits no jamming criticality [33]. This observation suggests that hyperuniformity, if intrinsic to the jamming transition, should likewise persist across a wide range of size ratios, up to the monodisperse limit. However, prior studies have reported that hyperuniformity disappears when the size ratio f_r is too small or too large [19, 29, 35]. It remains unclear whether hyperuniformity is genuinely absent at extreme size ratios, or whether it is present but obscured by spurious fluctuations. These fluctuations include local compositional fluctuations, which become prominent when f_r is very small, and noise from crystalline grain boundaries, which inevitably emerge as $f_r \rightarrow 1^-$. Existing variants of $S(q)$, such as the q -dependent isothermal compressibility $\chi_T(q)$ and the local volume fluctuation $\chi_V(q)$ mentioned above, do not sufficiently suppress these sources of noise or enhance the resolution needed to detect hyperuniformity.

To address this issue, we introduce a method inspired by Rissone *et al.* [36], originally developed for monodisperse systems. Their approach exploits the duality between particle centers and contact points in isostatic jammed networks. By shifting the representation from particle centers to contact points, they significantly enhanced the resolution for detecting long-range structural

correlations. This allowed for highly precise measurements of the hyperuniformity exponent, yielding $\alpha = 1$ in three-dimensional monodisperse systems. In this study, we adopt their method for bidisperse systems in two dimensions. Strictly speaking, this method cannot be applied to systems with size disparity, as the duality between particle centers and contact points no longer holds when the size ratio deviates from unity. Surprisingly, however, we find that this approach significantly improves the accuracy of the hyperuniformity exponent α , enabling robust characterization of hyperuniformity across a wide range of size ratios. Using this method, we show that the hyperuniformity exponent α for two-dimensional bidisperse systems consistently falls within the range $0.6 \lesssim \alpha \lesssim 0.7$ across the entire range of size ratios from the disparate value $f_r = 0.3$ up to nearly monodisperse systems $f_r \rightarrow 1^-$, excluding the singular case $f_r = 1$.

The remainder of this paper is organized as follows. In Sec. II, we describe the details of our simulation model and the protocol used to generate the jammed packings. In Sec. III, we outline the concepts underlying the contacts-based representation approach introduced by Rissone *et al.* [36] and our extension of this method to bidisperse systems. In Sec. IV, we present our numerical results. We conclude this paper in Sec. V.

II. SIMULATION MODEL

We study jammed packings of frictionless soft disks using molecular dynamics (MD) simulations [12, 13]. The system is a binary mixture of small and large particles with diameters σ_S and σ_L , respectively. We fix the number fraction at $f_N = N_S/(N_S + N_L) = 0.5$, where N_S and N_L denote the numbers of small and large particles. Most of the results presented below are based on systems with a total of $N = N_S + N_L = 4000$ particles. We also perform simulations with $N = 10000$ to confirm that our results are not affected by finite-size effects. To explore a broad range of structural orderings, we vary the particle size ratio $f_r = \sigma_S/\sigma_L$ from 0.3 to 1.0, following an approach similar to that used in previous studies [27, 29]. Here, $f_r = 1$ corresponds to a monodisperse system. The size ratio $f_r = 1/1.4 \approx 0.71$ is the most commonly used in studies of the jamming transition [12, 17]. The i -th and j -th particles interact via the harmonic potential defined by

$$U(r_{ij}) = \frac{\epsilon}{2} \left(1 - \frac{r_{ij}}{\sigma_{ij}}\right)^2 H\left(1 - \frac{r_{ij}}{\sigma_{ij}}\right), \quad (2)$$

where $r_{ij} = |\mathbf{r}_i - \mathbf{r}_j|$ is the inter-particle distance, $\sigma_{ij} = (\sigma_i + \sigma_j)/2$ is the average diameter of particles i and j , and $H(x)$ denotes the Heaviside step function. We use σ_S and ϵ as the units of length and energy, respectively.

To generate jammed packings, we first prepare a random configuration at a low packing fraction, $\varphi_{\text{ini}} = 0.835$.

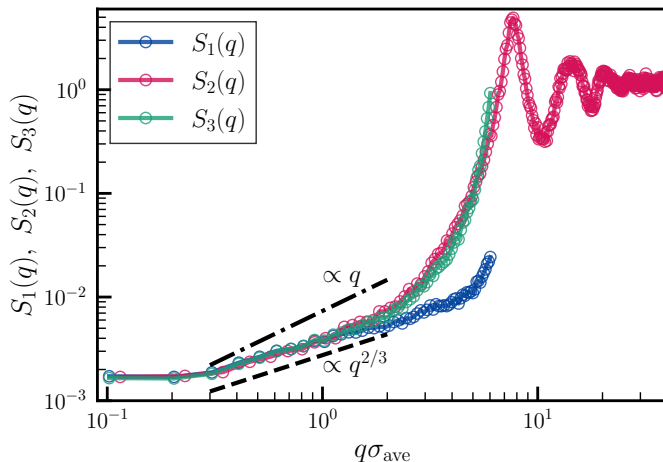


FIG. 1: Fourier-space measures of density fluctuations in the archetypal bidisperse jammed packings of $f_r = 0.71$ defined by Eqs. (3), (5), and (7).

The system is then compressed quasistatically with a packing fraction increment $\Delta\varphi$, which is gradually reduced from 2×10^{-3} to 10^{-6} as the jamming transition density φ_J is approached. After each compression step, the system is relaxed to a local energy minimum using the FIRE algorithm [37]. A configuration is considered jammed when the average potential energy per particle becomes nonzero, specifically when $N^{-1} \sum_{j>k} U(r_{jk}) > 10^{-16}$, which corresponds to $0 < (\varphi - \varphi_J) \leq 10^{-6}$. This is a protocol commonly used in the past [12] and closely resembles experimental procedures used in granular systems [38].

Let us recapitulate the hyperuniformity of the most commonly studied jammed system with a size ratio of $f_r = 1/1.4 \approx 0.71$, to demonstrate that the exponent α is indeed less than unity [26]. To this end, we compute several measures of density fluctuations introduced in previous studies, which generalize the structure factor $S(q)$ [2, 9, 17]. The first is the correlation function of the local volume fraction:

$$S_1(q) = \chi_V(q) = \frac{1}{V} \langle |\phi_1(\mathbf{q})|^2 \rangle. \quad (3)$$

Here, $\phi_1(\mathbf{q})$ is the Fourier transform of the local volume fraction defined as

$$\phi_1(\mathbf{r}) = \sum_i \Delta_i(\mathbf{r} - \mathbf{r}_i), \quad (4)$$

where $\Delta_i(\mathbf{r} - \mathbf{r}_i)$ is the indicator function, which is equal to 1 if \mathbf{r} lies within the i -th particle and 0 otherwise. The second is the correlation function

$$S_2(q) = \chi(q) = \frac{1}{V} \langle |\phi_2(\mathbf{q})|^2 \rangle, \quad (5)$$

defined in terms of an alternative local volume fraction $\phi_2(\mathbf{q})$, whose real-space definition is given by

$$\phi_2(\mathbf{r}) = \sum_i v_i \delta(\mathbf{r} - \mathbf{r}_i), \quad (6)$$

where $v_i = \pi\sigma_i^2/4$ is the area of the i -th particle. The third measure is the wavenumber-dependent isothermal compressibility, defined for bidisperse systems by

$$S_3(q) = \chi_T(q) = \frac{S_{SS}(q)S_{LL}(q) - S_{LS}^2(q)}{\frac{N_S^2}{N^2}S_{LL}(q) + \frac{N_L^2}{N^2}S_{SS}(q) - 2\frac{N_S N_L}{N^2}S_{LS}(q)}, \quad (7)$$

where $S_{\nu\mu}(q) = N^{-1} \langle \delta\rho_\nu(\mathbf{q})\delta\rho_\mu^*(\mathbf{q}) \rangle$ ($\nu, \mu = S, L$) is the static structure matrix for a binary mixture, and $\rho_\nu(\mathbf{q})$ is the density of the component ν [16, 26].

In Fig. 1, we show all $S_i(q)$ ($i = 1, 2, 3$) for $f_r = 0.71$. It is evident that the hyperuniformity exponent α is not 1, but is instead well fitted by $\alpha = 0.6-0.7$, as reported in Ref. [26]. We believe that the exponent should be $\alpha = 2/3$, which we shall rationalize below. Figure 1 also demonstrates that, at large length scales ($q\sigma_{\text{ave}} \lesssim 2$), the density fluctuations are largely independent of the specific definition of $S_i(q)$.

Given this consistency, we shall use $S_2(q)$ (Eq. (5)) as the reference structure factor for comparison with our new observable throughout the remainder of the paper, referring to it simply as $S(q)$.

In the following, we also compute the fluctuations of the local volume fraction,

$$\sigma_\varphi^2(R) = \langle \varphi^2(R) \rangle - \langle \varphi(R) \rangle^2, \quad (8)$$

where $\varphi(R) = V_R^{-1} \int_{V_R} \phi_2(\mathbf{r}) d\mathbf{r}$ is the packing fraction within a circular region of radius R and area V_R . For hyperuniform systems, with $S(q) \propto q^\alpha$ as $q \rightarrow 0$, the large- R behavior of $\sigma_\varphi^2(R)$ is [2]

$$\sigma_\varphi^2(R) \propto R^{-d-\alpha}, \quad (\alpha < 1). \quad (9)$$

III. GENERALIZATION OF CONTACTS-BASED REPRESENTATION

Hyperuniformity is characterized by suppressed density fluctuations at large length scales. However, its analysis in jamming systems is hindered by statistical noise, overlapping signals, and finite-size effects, which make accurate characterization near the jamming transition challenging [17, 22, 36].

Rissone *et al.* [36] recently proposed a method to compute real-space correlation functions at long distances with high accuracy. This approach exploits the dual relationship between particle centers and their contact points with neighboring particles. In this *contacts-based representation*, one considers the contact points as *quasi-particles* of effective diameter $\sigma' = \sigma/2$, where σ is the particle diameter. This representation enhances structural features hidden in traditional particle-based descriptions. By analyzing the contact-contact correlation function in three-dimensional monodisperse systems, Rissone *et al.* found a power-law decay in the radial distribution function, $g(r) \propto r^{-\gamma}$, with an exponent $\gamma \approx 4$. Since $S(q)$ is the Fourier transform of $g(r)$ and the hyperuniformity exponent α in Eq. (1) is related to γ via

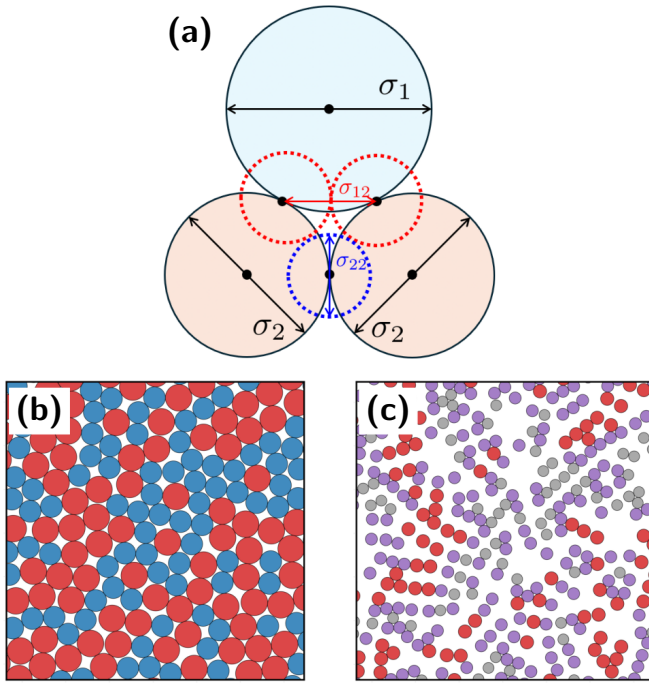


FIG. 2: (a) Schematic of the contacts-based representation in a bidisperse jammed packing. Three real particles in mutual contact form a locally dense configuration. Quasi-particles (dashed circles) are centered at contact points, with effective diameters given by Eq. (11). (b) Portion of a jammed configuration with real particles at size ratio $f_r = 0.82$. (c) Corresponding contacts-based representation with quasi-particles located at the contact points of (b). Colors indicate relative particle diameters.

$\alpha = \gamma - d$, their results correctly reproduce $\alpha = 1$ for $d = 3$ [21]. The authors further suggested that other contact-related observables, such as contact forces or moments of the contact number, may enhance the precision of long-range correlation measurements, thereby improving the accuracy of the hyperuniformity exponent.

However, this method is limited to monodisperse systems, where a rigorous duality exists between contact points and particle centers. This duality breaks down in systems with size dispersity, including the bidisperse systems considered here. Such dispersity is essential for generating disordered jammed packings in two dimensions, as monodisperse systems tend to crystallize even under infinitely rapid compression. Nevertheless, we postulate that the distribution of contact points may be less susceptible to unwanted fluctuations than that of particle centers. Therefore, we adopt the contacts-based representation from Rissone *et al.* without modification and apply it to our bidisperse systems. In this representation, *quasi-particles* are placed at the contact points between real particles. Figure 2 provides a schematic illustration of these quasi-particles, centered at the points where real particles kiss. The contact point between the i -th and

j -th particles is denoted by (ij) . To study density fluctuations in this framework, we assign each quasi-particle a volume

$$v_{ij} = \frac{\pi \sigma_{ij}^2}{4}, \quad (10)$$

where σ_{ij} is its effective diameter. The definition of σ_{ij} can be adjusted to reflect specific physical scaling properties. In monodisperse systems, Rissone *et al.* weighted quasi-particles by the inverse of interparticle forces or by fluctuations in contact number [36]. For our analysis of large-scale density fluctuations, we define the effective diameter as

$$\frac{1}{\sigma_{ij}} \equiv \frac{1}{\sigma_i} + \frac{1}{\sigma_j}, \quad (11)$$

where σ_i and σ_j denote the diameters of the particles in contact at the center of the quasi-particle. Our choice of σ_{ij} is motivated by the geometric interpretation of void space in jammed packings. Following Zachary *et al.* [9], hyperuniformity arises from the homogenization of voids bounded by contact points, which serve as centers of quasi-particles. Thus, studying the distribution of volumes associated with these quasi-particles effectively probes void space uniformity. Equation (11) appropriately weights contacts involving larger particles, reflecting their greater influence on density correlations. While this definition does not exactly capture inter-quasi-particle distances, especially in polydisperse systems, Appendix A shows it provides a good estimate of typical spacing and that alternative formulas yield negligible differences for the size ratios considered. Notably, as $f_r \rightarrow 1^-$ in the monodisperse limit, sensitivity to the precise form of σ_{ij} diminishes. Analogous to the structure factor for real particles with size disparity defined in Eq. (5), we define the structure factor of quasi-particles in the contacts-based representation as

$$S_c(q) = \frac{1}{V} \left\langle \left| \sum_{(ij)} v_{ij} e^{-i\mathbf{q} \cdot \mathbf{r}_{ij}} \right|^2 \right\rangle, \quad (12)$$

where the sum runs over all contact points (ij) , with v_{ij} representing the volume of quasi-particles, as defined by Eq. (10).

Our contacts-based representation is constructed from jammed configurations of real particles by iteratively removing all *rattlers*, defined as particles with fewer than $d + 1 = 3$ contacts, until none remain. Depending on the size ratio f_r , rattlers constitute approximately 5% to 20% of the system. For the range of f_r studied, the generated bidisperse packings are close to the jamming transition and isostatic, with an average contact number per non-rattler particle $\langle z_i \rangle \approx z_{\text{iso}} = 2d = 4$. This yields approximately $2N_{\text{non-rattlers}} \approx 2N$ contact points. Consequently, the quasi-particle system defined by these contact points is substantially larger than the original particle system.

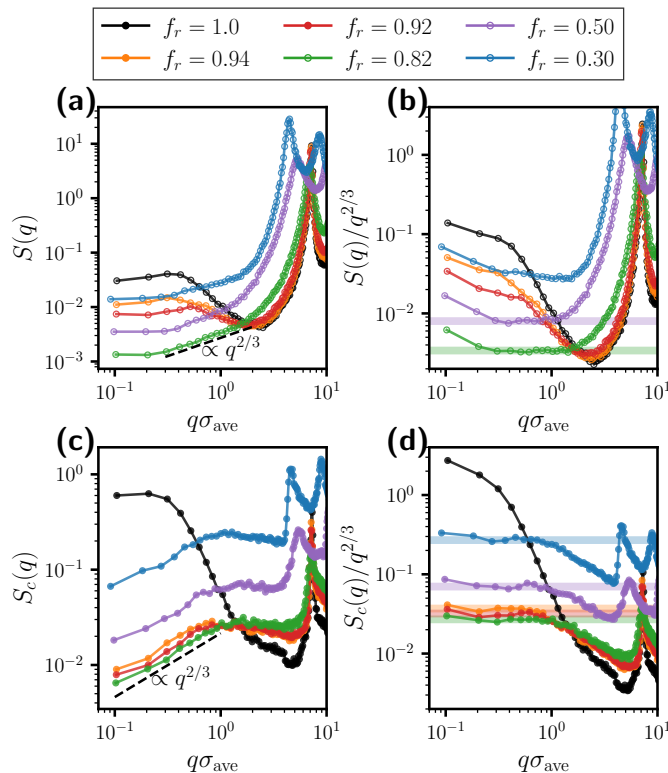


FIG. 3: (a) Structure factor $S(q) = S_2(q)$ of real particles for various size ratios f_r . (b) Same data as in (a), rescaled by $q^{2/3}$. (c) Structure factor $S_c(q)$ of quasi-particles in the contacts-based representation for the same f_r values. (d) Rescaled $S_c(q)/q^{2/3}$ highlighting the low- q plateau. Horizontal lines serve as visual guides.

IV. RESULTS

The jamming transition density φ_J , contact number, structural order, and mechanical response vary significantly with the composition of the mixture, such as the number fraction f_N and size ratio f_r [27–29]. Here, we investigate the dependence of hyperuniformity on the size ratio f_r over a broad range by fixing the number fraction at $f_N = 0.5$.

Introducing bidispersity into crystalline monodisperse disk packings distorts the contact network: contacts are broken, and particles are displaced from their crystalline positions. These changes, however, are subtle and often difficult to detect in the real particle configurations when $f_r \rightarrow 1^-$. This suggests that the contacts-based representation, which is more sensitive to variations in the contact network and jamming-related features, provides a more effective framework for probing long-range density correlations. Indeed, Tong *et al.* [33] showed that weak polydispersity can significantly alter the contact number distribution—and consequently the distribution of quasi-particles in the contacts-based representation—even though the real particle arrangement re-

mains nearly crystalline. However, it remains unclear whether our extension of the contacts-based representation to bidisperse systems retains the same advantages in quantifying hyperuniformity as observed in monodisperse packings. Following the procedure outlined in Sec. III, we investigate the structure factor of quasi-particles defined by Eq. (12), in addition to that of real particles.

Figure 3 (a) shows the structure factor $S(q)$ of real particles, defined by Eq. (5) and measured using the conventional method, for various size ratios f_r . For moderate size ratios $f_r = 0.5$ and 0.82 , we observe hyperuniformity with an exponent $\alpha = 0.6$ – 0.7 , similar to the case of $f_r = 0.71$ shown in Fig. 1. However, the algebraic behavior is less distinct for other values of f_r . In particular, as f_r increases, $S(q)$ exhibits a clear enhancement at small wavenumbers q . The hyperuniform behavior is completely absent for $f_r = 0.92$ (red), 0.94 (orange), and for the monodisperse system $f_r = 1.0$ (black).

Figure 4 presents selected regions of jammed packings for several values of f_r . The left panels show the configurations of real particles, with colors representing the Tong–Tanaka local packing order parameter for each particle [39]. This order parameter for the i -th particle is defined as

$$\Theta_i = \frac{1}{N_i} \sum_{\langle jk \rangle} \left| \theta_{jk}^{(1)} - \theta_{jk}^{(2)} \right|, \quad (13)$$

where N_i is the number of neighboring particle pairs $\langle jk \rangle$ adjacent to the i -th particle, $\theta_{jk}^{(1)}$ is the angle between \mathbf{r}_{ij} and \mathbf{r}_{ik} formed by each such pair, and $\theta_{jk}^{(2)}$ is the corresponding angle when the three particles are perfectly in contact. This parameter quantifies local packing efficiency: particles shown in blue are more densely packed, and particles shown in red are more loosely packed. The right panels show the corresponding quasi-particle configurations derived from the contact networks in the left panels. Here, the colors indicate the effective diameters calculated from Eq. (11) of the quasi-particles relative to the smallest quasi-particle diameter, $\sigma_S/2$. From the configurations of real particles, we observe that packings with moderate size ratios such as $f_r = 0.82$ exhibit no evident structural order, and the particles are not efficiently packed. Therefore, these systems are expected to exhibit the hyperuniformity typical of disordered jammed packings, as confirmed in Fig. 3 (a). In contrast, for systems with size ratios approaching the monodisperse limit ($f_r \rightarrow 1^-$), such as $f_r = 0.94$, and in the monodisperse case ($f_r = 1.0$), particles form crystalline domains. The emergence of polycrystalline domain boundaries and fluctuations in domain sizes lead to an enhancement at small wavenumbers q , as reflected in the behavior of $S(q)$.

Note that jamming criticality, such as $\delta z \propto \delta \varphi^{1/2}$, persists even in the nearly monodisperse regime ($f_r \rightarrow 1^-$) [33, 34]. The enhancement of $S(q)$ at large f_r , which masks the underlying hyperuniformity, is attributed to the formation of grain boundaries associated with crystalline ordering, as noted above. The typical

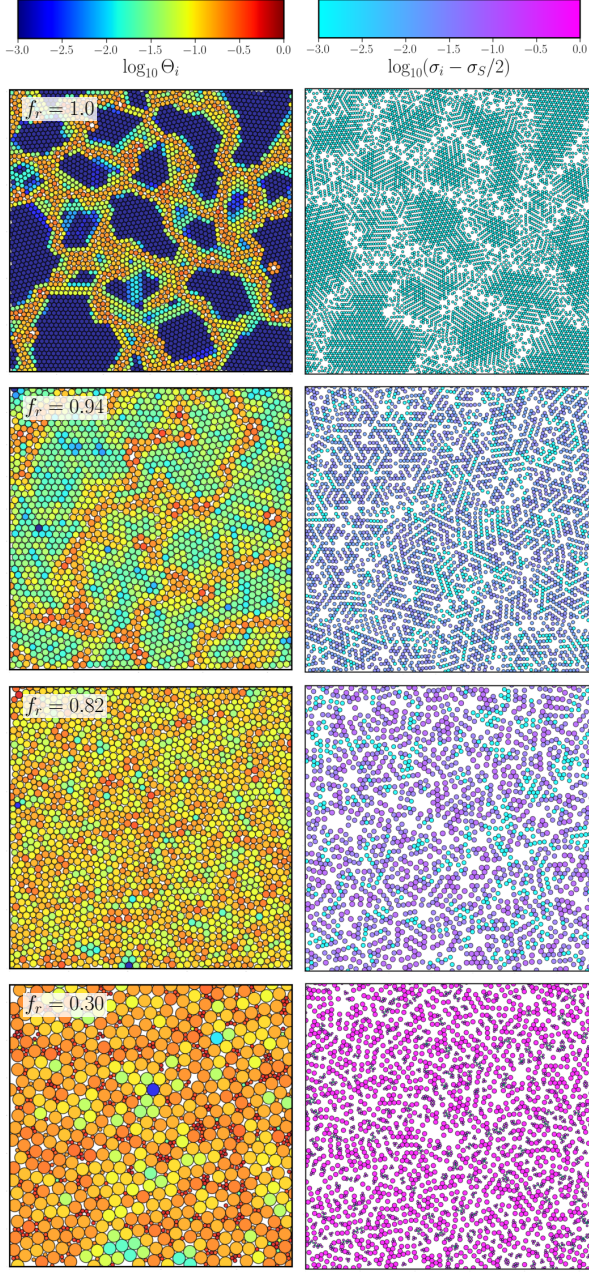


FIG. 4: Snapshot of selected regions of jammed configurations. The size ratio f_r decreases from top ($f_r = 1.0$) to bottom ($f_r = 0.3$). Left: real particles, colored by the Tong-Tanaka structural order parameter [39]. Right: quasi-particles in the corresponding contacts-based representation, colored by diameters defined in Eq. (11).

size of polycrystalline domains can be estimated from the structure factors in Fig. 3 (a). The domain size is given by $L_d = 2\pi/q_d$, where q_d denotes the wavenumber below which $S(q)$ shows enhancement. These estimates are consistent with the structural domain sizes observed in Fig. 4. For instance, we find $L_d \approx 8\sigma_{\text{ave}}$ for $f_r = 0.94$.

Let us now turn our attention to the contacts-based

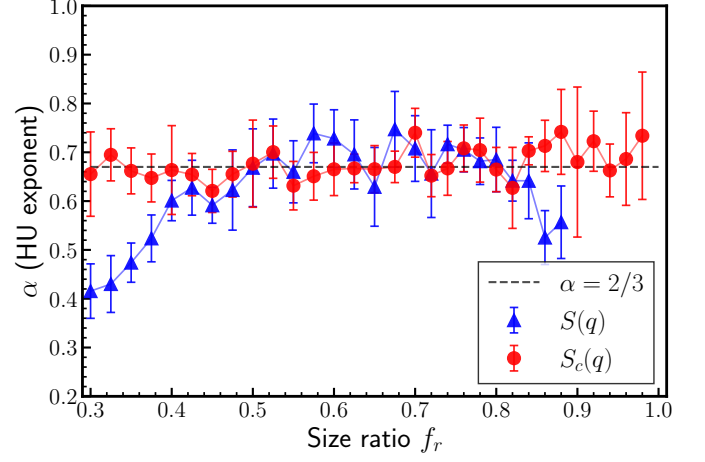


FIG. 5: The hyperuniformity exponent α measured from the structure factor of the real particles [Eq. (5), blue] and of the quasi-particles [Eq. (12), red]. The dashed line indicates the predicted value $\alpha = 2/3$.

representation. Figure 3 (c) shows the structure factor $S_c(q)$ defined by Eq. (12) for quasi-particles in this representation. Remarkably, $S_c(q)$ decays toward zero as $q \rightarrow 0$ for all f_r in the range $0.3 \leq f_r \leq 0.94$, following a power law $S_c(q) \propto q^\alpha$ with exponent close to $2/3$, indicating the robustness of hyperuniformity. To highlight the improved accuracy of $S_c(q)$ relative to $S(q)$, we plot both $S(q)$ and $S_c(q)$ rescaled by $q^{2/3}$ in Figs. 3 (b) and 3 (d), respectively. Both quantities exhibit a plateau at small q for moderate size ratios $0.5 \leq f_r \leq 0.8$. However, for systems near the monodisperse limit ($f_r > 0.92$) and for strongly size-disparate systems ($f_r = 0.3$), $S(q)/q^{2/3}$ shows significant enhancement at low q , deviating from the expected scaling. In contrast, $S_c(q)/q^{2/3}$ maintains a plateau across the entire range of f_r studied, except for the monodisperse system $f_r = 1.0$. Furthermore, the q -window over which the plateau is observed is consistently broader for $S_c(q)$ than for $S(q)$. Even for moderate size ratios $0.5 \leq f_r \leq 0.82$, where hyperuniformity is most evident, $S(q)$ for real particles exhibits saturation below $q^*\sigma_{\text{ave}} \approx 0.2$, indicating a finite length scale associated with the breakdown of hyperuniform scaling. No such saturation is evident in $S_c(q)$. It is premature to conclude that the system is ideally hyperuniform, as a faint upturn in $S_c(q)$ is also visible for $q < q^*$ in Fig. 3 (d). However, it is safe to conclude that the contacts-based analysis provides a superior characterization compared to the real particle representation, with hyperuniform long-range correlations persisting robustly up to nearly the monodisperse limit. The monodisperse packing ($f_r = 1.0$) remains an exception, where both $S(q)$ and $S_c(q)$ consistently show low- q enhancement, indicating a finite domain size of $L_d \approx 15\sigma_{\text{ave}}$.

To quantify hyperuniformity across different size ratios f_r , we fit the power-law form in Eq. (1) to the structure factors $S(q)$ of real particles and $S_c(q)$ of quasi-particles

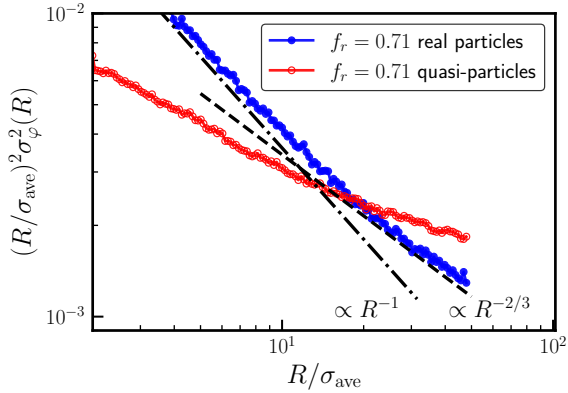


FIG. 6: Local volume fluctuation for the disordered jammed system with $f_r = 0.71$ and $N = 10\,000$.

in the contacts-based representation. Because the exponent α is sensitive to the fitting range, we select intervals of wavenumber q where variations in the fitting range have minimal effect on α [35]. Figure 5 shows the values of α obtained from both $S(q)$ and $S_c(q)$ over the entire range of f_r from 0.3 to 1. The α values derived from $S(q)$ exhibit a non-monotonic dependence on f_r : they start as low as 0.4, peak near 0.7 for moderate size ratios ($f_r = 0.5$ – 0.8), and then decrease as f_r approaches the monodisperse limit at 1. In contrast, α values extracted from $S_c(q)$ remain nearly constant, fluctuating around $2/3$ throughout the entire range of f_r .

Finally, we investigate the real-space fluctuations of the local volume fraction, as defined in Eq. (8), for both real and quasi-particles. In systems with a hyperuniformity exponent $\alpha < 1$, the real-space signature of hyperuniformity is the anomalous suppression of local volume fraction fluctuations, characterized by the scaling relation $R^2 \sigma_\phi^2(R) \propto R^{-\alpha}$ [2]. To suppress statistical noise and mitigate finite-size effects, we adopt the method of Dreyfus *et al.* [19], in which the original configuration is replicated in a 3×3 tiling to construct a larger fictitious system. This stitched configuration remains jammed due to periodic boundary conditions. Figure 6 shows the local volume fraction fluctuations for the size ratio $f_r = 1/1.4 \approx 0.71$ and system size $N = 10^4$. The results are somewhat puzzling. For real particles (blue dots), the rescaled fluctuations $R^2 \sigma_\phi^2(R)$ decay as R^{-1} at intermediate length scales, transitioning to a slower decay, approximately $R^{-0.6}$, at larger scales ($R > 30$). This confirms that $\alpha \approx 0.6$, consistent with the results obtained from $S(q)$. In contrast, the quasi-particles in the contacts-based representation exhibit an even weaker exponent, $\alpha = 0.4$ – 0.5 , at the largest R . This discrepancy between the large- R scaling of real-space fluctuations and the small- q scaling in Fourier space might be attributed to short-range correlations, which can persist and influence volume fraction fluctuations even at large R [17]. Therefore, the Fourier-space structure factors $S(q)$ and

$S_c(q)$ provide a more reliable and robust characterization of hyperuniformity, which is the approach adopted throughout this study.

V. CONCLUSIONS AND DISCUSSION

In this work, we investigated hyperuniformity in two-dimensional jammed packings, focusing on its dependence on bidispersity. Hyperuniformity is characterized by a vanishing structure factor, $S(q) \propto q^\alpha$ with $\alpha > 0$ as $q \rightarrow 0$. We examined this behavior both in the spatial distribution of real particles and in that of quasi-particles centered at contact points. Across a wide range of size ratios, we consistently observed hyperuniformity with exponent $\alpha = 0.6$ – 0.7 , in agreement with our previous results for the classic 1:1.4 equimolar binary mixture [26]. Hyperuniformity is more clearly observed in the contacts-based representation, particularly near the monodisperse limit where local crystalline order in real particle configurations masks long-range correlations. In contrast, the quasi-particle framework reveals robust hyperuniform behavior with $\alpha \approx 2/3$ across all bidisperse systems, except for the ideal triangular crystal. These findings underscore the importance of the contacts-based approach in capturing long-range structural features and demonstrate its utility for probing hyperuniformity in jammed systems beyond the reach of conventional particle-based analyses.

In hindsight, the exponent $\alpha = 2/3$ should not be considered surprising, given the mean-field nature of the jamming transition [26]. The upper critical dimension of the jamming transition is $d_c = 2$ [14, 40]. In the thermodynamic limit, the fluctuation of the local volume fraction, $\sigma_\phi^2(R)$, measured in subsystems of volume R^d , is asymptotically proportional to the fluctuation of the global packing fraction, $\langle \delta\varphi_J^2 \rangle \equiv \langle (\varphi_J - \langle \varphi_J \rangle_{R=\infty})^2 \rangle$, up to a constant factor [41]. O’Hern *et al.* analyzed the system size dependence of the distribution of the global packing fraction and found that

$$\langle \delta\varphi_J^2 \rangle \propto N^{-\Omega} \propto R^{-d\Omega}. \quad (14)$$

with the exponent Ω independent of dimension d [12]. If $\langle \delta\varphi_J^2 \rangle \propto \sigma_\phi^2(R)$, we conclude $\sigma_\phi^2(R) \propto R^{-d\Omega}$. Comparing this with Eq. (9), we arrive at $\alpha = d(\Omega - 1)$. If Ω is independent of d and $\alpha = 1$ for $d = 3$, we expect $\alpha = 2/3$ for $d = 2$, consistent with our simulation results.

Our results are obtained for typical random close packings (RCPs) generated via a standard compression protocol. These jammed configurations represent the ensemble of states most likely generated by uniformly compressing a random initial configuration to the jamming point [18]. Consequently, the exponent $\alpha \approx 2/3$ reported here does not conflict with hyperuniformity exponents obtained for maximally random jammed (MRJ) packings—defined by geometric rather than entropic criteria—produced by alternative protocols: $\alpha = 1$ from the Lubachevsky–Stillinger algorithm [8, 9], $\alpha \approx 0.45$ from

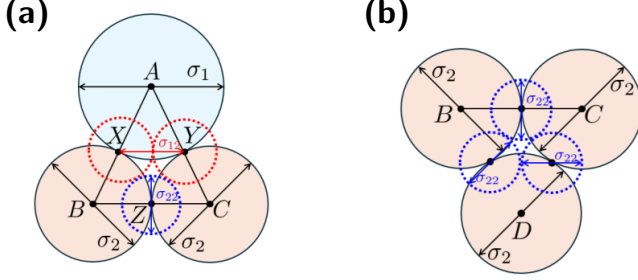


FIG. A1: Schematic representation of the quasi-particles (dashed circles) located at contact points of real particles (solid circles) for binary systems in two scenarios (a) and (b).

the Torquato–Jiao algorithm [42], and even larger values ($\alpha = 2$ or 4) from tessellation-based approaches [43].

The present findings highlight the connection between long-range density fluctuations and jammed states, although the precise relationship with hyperuniformity remains unresolved [22, 44]. Hexner *et al.* [45] proposed that the suppression of fluctuations in the excess contact number signals diverging length scales near the jamming transition. Nevertheless, the exact origin of hyperuniformity of the density at the jamming transition and its relation to the associated critical behavior remain open questions, warranting further investigation.

ACKNOWLEDGMENTS

This work was supported by KAKENHI (Grant Numbers JP20H00128, JP22H04472, JP23H04503, JP24H00192), and the JST FOREST Program (Grant Number JPMJFR212T).

Appendix A: Diameter of Quasi-particles: a geometrical argument

In this appendix, we justify our choice of the effective diameter for the quasi-particles, as given by Eq. (11). In Sec. III, we introduced a contacts-based representation centered on the contact points between particles, rather than their centers. This representation consists of *quasi-particles* located at the contact points of the real particles. Figure A1 illustrates this concept in a small subregion of the jammed configuration, highlighting the densest packing among three particles. Since our system is binary, only two scenarios are possible, as shown in Figs. A1 (a) and (b).

We first focus on the scenario illustrated in Fig. A1 (a). Real particles with centers at points A, B, and C, and radii σ_1 , σ_2 , and σ_2 , respectively, are mutually in contact. Since the system is just above the jamming transition, it

is reasonable to assume negligible overlap between particles. The contact points are denoted by X, Y, and Z. In the contacts-based representation, to account for size disparity and accurately probe density fluctuations, the effective diameter assigned to each quasi-particle must ensure that the quasi-particles just touch one another at the jamming transition. This choice appropriately reflects the occupied volume of each contact point in the jammed configuration and equivalently represents the void space bounded by these contacts. In the case of Fig. A1 (a), by symmetry, the radii of the quasi-particles centered at points X and Y are both σ_{12} . Applying Thales's theorem to the segment $XY \parallel BC$, we obtain

$$\frac{\sigma_{12}}{\sigma_2} = \frac{XY}{BC} = \frac{AX}{AB} = \frac{\sigma_1}{\sigma_1 + \sigma_2}. \quad (\text{A1})$$

This implies that the diameter of the quasi-particles centered at X and Y is

$$\sigma_{12} = \frac{\sigma_1 \sigma_2}{\sigma_1 + \sigma_2}, \quad (\text{A2})$$

which precisely matches the effective diameter definition proposed for the quasi-particles in Eq. (11). Given this, the diameter of the quasi-particle centered at Z can be determined to ensure that the three quasi-particles are mutually in contact. To do so, we observe that

$$\frac{\sigma_2}{\sigma_1 + \sigma_2} = \cos(\angle ABC) = 1 - 2 \sin^2 \left(\frac{\angle ABC}{2} \right) \quad (\text{A3})$$

and

$$\sin \left(\frac{\angle ABC}{2} \right) = \sqrt{\frac{\sigma_1}{2(\sigma_1 + \sigma_2)}}. \quad (\text{A4})$$

Then, the diameter σ_{22} of the quasi-particle whose center is at Z is

$$\begin{aligned} \sigma_{22}^{(a)} &= 2XZ - \sigma_{12} \\ &= 2\sigma_2 \sin \left(\frac{\angle ABC}{2} \right) - \frac{\sigma_1 \sigma_2}{\sigma_1 + \sigma_2} \\ &= \frac{\sigma_2}{2} \left(2\sqrt{\frac{2\sigma_1}{\sigma_1 + \sigma_2}} - \frac{2\sigma_1}{\sigma_1 + \sigma_2} \right). \end{aligned} \quad (\text{A5})$$

We confirm that in the monodisperse case, where $\sigma_1 = \sigma_2 = \sigma$, Eq. (A5) yields the same value, $\sigma/2$, as proposed by Rissone *et al.* [36]. A subtlety regarding Eqs. (11) and (A2) should be noted: the diameter of a quasi-particle in these two equations is determined solely by the diameters of the two real particles in contact. In contrast, Eq. (A5) depends on the diameters of three mutually contacting particles. Thus, for each triplet of mutually contacting particles, there is a unique assignment of effective diameters to the quasi-particles.

Now, consider the scenario in Fig. A1 (b), where identical real particles of diameter σ_2 , centered at points B and C, are in contact, and each is also in contact with another identical particle centered at D. By symmetry,

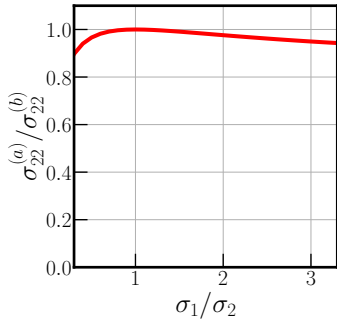


FIG. A2: The difference between the effective diameter of quasi-particles calculated from Eq. (A5) and from Eq. (A6) in the range of size ratio we investigated.

the effective diameter of the three quasi-particles (blue dashed circles) is given by

$$\sigma_{22}^{(b)} = \frac{\sigma_2}{2}, \quad (\text{A6})$$

consistent with the result obtained by Rissone *et al.* for monodisperse systems [36]. Thus, if we combine the scenarios in Fig. A1 (a) and (b), such that the real particles B and C of diameter σ_2 are in contact and each also contacts both the real particle A of diameter σ_1 and the particle D of diameter σ_2 , then the diameter of the quasi-particle located at the contact point between B and C can be determined using either Eq. (A5) or Eq. (A6). These two expressions yield different values, indicating a form of geometrical frustration. In other words, when $\sigma_1 \neq \sigma_2$, there is no unique assignment of effective quasi-particle diameters that ensures all quasi-particles are just in contact at the jamming transition.

However, since our work focuses on systems with size ratios $f_r > 0.3$, the choice of Eq. (A2) for the effective quasi-particle diameter is appropriate for all quasi-particles. It has been shown that in systems with extreme size disparities (typically $f_r < 0.15$), small particles become rattlers that fit within voids formed by large particles without interacting with others [27]. These extreme cases exhibit nontrivial behaviors, including hyperstatic packings ($z > z_{\text{iso}}$) and anomalously large bulk moduli comparable to crystalline configurations. Such systems differ markedly from disordered jamming and are thus beyond the scope of this study. The results presented here are for systems with $0.3 \leq f_r \leq 1.0$, corresponding to a size ratio range between any two particles of $0.3 \leq \sigma_1/\sigma_2 \leq 3.3$. Within this range, the difference between Eq. (A5) and Eq. (A6) is less than 15%, as shown in Fig. A2. This discrepancy introduces an error in the hyperuniformity exponent α smaller than the error bars in Fig. 5, and is therefore negligible. In summary, σ_{12} defined by Eq. (A2) is an appropriate effective diameter for quasi-particles in the contacts-based representation within the size ratio range where conventional disordered jamming behavior occurs.

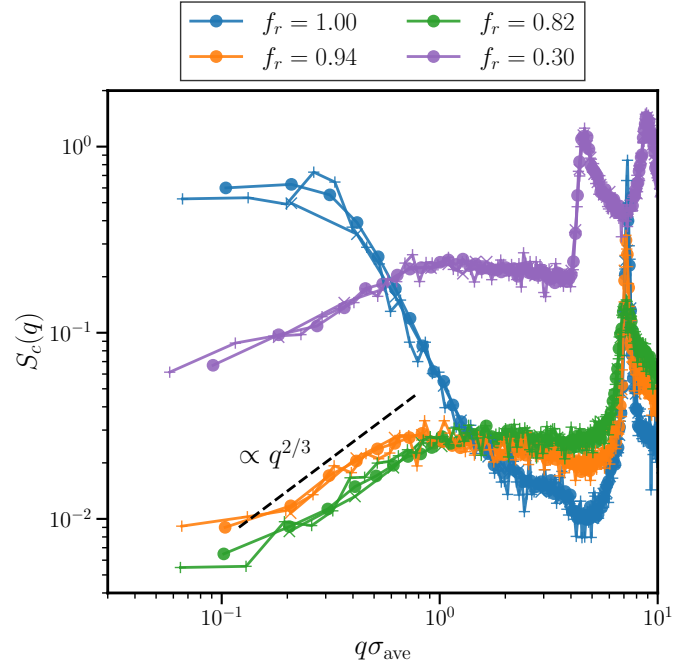


FIG. B1: The structure factor $S_c(q)$ of the quasi-particles for $N = 1000(\times)$, $N = 4000(o)$, $N = 10000(+)$ for equimolar bidisperse system with various size ratios f_r .

Appendix B: System size dependence

Figure B1 shows the structure factor of quasi-particles for systems of different sizes, $N = 1000, 4000$, and 10000 . Due to periodic boundary conditions, larger systems provide access to smaller wavenumbers, with $q_{\text{min}} \propto 1/\sqrt{N}$. We observe that the structure factors collapse onto a single curve, indicating that the hyperuniformity measured in the contacts-based representation is independent of system size.

-
- [1] S. Torquato and F. H. Stillinger, Local density fluctuations, hyperuniformity, and order metrics, *Phys. Rev. E* **68**, 041113 (2003).
 - [2] S. Torquato, Hyperuniform states of matter, *Physics Reports* **745**, 1 (2018).
 - [3] A. Gabrielli, M. Joyce, and F. Sylos Labini, Glass-like universe: Real-space correlation properties of standard cosmological models, *Phys. Rev. D* **65**, 083523 (2002).
 - [4] Y. Jiao, T. Lau, H. Hatzikirou, M. Meyer-Hermann, J. C. Corbo, and S. Torquato, Avian photoreceptor patterns represent a disordered hyperuniform solution to a multi-scale packing problem, *Phys. Rev. E* **89**, 022721 (2014).
 - [5] A. Mayer, V. Balasubramanian, T. Mora, and A. M. Walczak, How a well-adapted immune system is organized, *Proceedings of the National Academy of Sciences* **112**, 5950 (2015), <https://www.pnas.org/doi/pdf/10.1073/pnas.1421827112>.
 - [6] G. Zhang, F. H. Stillinger, and S. Torquato, The perfect glass paradigm: Disordered hyperuniform glasses down to absolute zero, *Scientific Reports* **6**, 36963 (2016).
 - [7] A. Donev, S. Torquato, and F. H. Stillinger, Pair correlation function characteristics of nearly jammed disordered and ordered hard-sphere packings, *Phys. Rev. E* **71**, 011105 (2005).
 - [8] C. E. Zachary, Y. Jiao, and S. Torquato, Hyperuniform long-range correlations are a signature of disordered jammed hard-particle packings, *Phys. Rev. Lett.* **106**, 178001 (2011).
 - [9] C. E. Zachary, Y. Jiao, and S. Torquato, Hyperuniformity, quasi-long-range correlations, and void-space constraints in maximally random jammed particle packings. i. polydisperse spheres, *Phys. Rev. E* **83**, 051308 (2011).
 - [10] S. Atkinson, G. Zhang, A. B. Hopkins, and S. Torquato, Critical slowing down and hyperuniformity on approach to jamming, *Phys. Rev. E* **94**, 012902 (2016).
 - [11] A. J. Liu and S. R. Nagel, Jamming is not just cool any more, *Nature* **396**, 21 (1998).
 - [12] C. S. O'Hern, L. E. Silbert, A. J. Liu, and S. R. Nagel, Jamming at zero temperature and zero applied stress: The epitome of disorder, *Phys. Rev. E* **68**, 011306 (2003).
 - [13] M. van Hecke, Jamming of soft particles: geometry, mechanics, scaling and isostaticity, *Journal of Physics: Condensed Matter* **22**, 033101 (2009).
 - [14] Wyart, M., On the rigidity of amorphous solids, *Ann. Phys. Fr.* **30**, 1 (2005).
 - [15] P. Charbonneau, J. Kurchan, G. Parisi, P. Urbani, and F. Zamponi, Fractal free energy landscapes in structural glasses, *Nature Communications* **5**, 3725 (2014).
 - [16] L. Berthier, P. Chaudhuri, C. Coulais, O. Dauchot, and P. Sollich, Suppressed compressibility at large scale in jammed packings of size-disperse spheres, *Phys. Rev. Lett.* **106**, 120601 (2011).
 - [17] Y. Wu, P. Olsson, and S. Teitel, Search for hyperuniformity in mechanically stable packings of frictionless disks above jamming, *Phys. Rev. E* **92**, 052206 (2015).
 - [18] S. Atkinson, F. H. Stillinger, and S. Torquato, Existence of isostatic, maximally random jammed monodisperse hard-disk packings, *Proceedings of the National Academy of Sciences* **111**, 18436 (2014), <https://www.pnas.org/doi/pdf/10.1073/pnas.1408371112>.
 - [19] R. Dreyfus, Y. Xu, T. Still, L. A. Hough, A. G. Yodh, and S. Torquato, Diagnosing hyperuniformity in two-dimensional, disordered, jammed packings of soft spheres, *Phys. Rev. E* **91**, 012302 (2015).
 - [20] A. T. Chieco, M. Zu, A. J. Liu, N. Xu, and D. J. Durian, Spectrum of structure for jammed and unjammed soft disks, *Phys. Rev. E* **98**, 042606 (2018).
 - [21] A. Donev, F. H. Stillinger, and S. Torquato, Unexpected density fluctuations in jammed disordered sphere packings, *Phys. Rev. Lett.* **95**, 090604 (2005).
 - [22] M. Ozawa, L. Berthier, and D. Coslovich, Exploring the jamming transition over a wide range of critical densities, *SciPost Phys.* **3**, 027 (2017).
 - [23] S. Torquato, T. M. Truskett, and P. G. Debenedetti, Is random close packing of spheres well defined?, *Phys. Rev. Lett.* **84**, 2064 (2000).
 - [24] A. Ikeda, L. Berthier, and G. Parisi, Large-scale structure of randomly jammed spheres, *Phys. Rev. E* **95**, 052125 (2017).
 - [25] N. Xu and E. S. C. Ching, Effects of particle-size ratio on jamming of binary mixtures at zero temperature, *Soft Matter* **6**, 2944 (2010).
 - [26] H. Matsuyama, M. Toyoda, T. Kurahashi, A. Ikeda, T. Kawasaki, and K. Miyazaki, Geometrical properties of mechanically annealed systems near the jamming transition, *The European Physical Journal E* **44**, 133 (2021).
 - [27] D. J. Koeze, D. Vågberg, B. B. T. Tjoa, and B. P. Tighe, Mapping the jamming transition of bidisperse mixtures, *Europhysics Letters* **113**, 54001 (2016).
 - [28] K. Saitoh and B. P. Tighe, Jamming transition and normal modes of polydisperse soft particle packing, *Soft Matter* **21**, 1263 (2025).
 - [29] J. Ricouvier, R. Pierrat, R. Carminati, P. Tabeling, and P. Yazhgur, Optimizing hyperuniformity in self-assembled bidisperse emulsions, *Phys. Rev. Lett.* **119**, 208001 (2017).
 - [30] C. P. Goodrich, A. J. Liu, and S. R. Nagel, Solids between the mechanical extremes of order and disorder, *Nature Physics* **10**, 578 (2014).
 - [31] T. Kawasaki and K. Miyazaki, Unified understanding of nonlinear rheology near the jamming transition point, *Phys. Rev. Lett.* **132**, 268201 (2024).
 - [32] D. Pan, Y. Wang, H. Yoshino, J. Zhang, and Y. Jin, A review on shear jamming, *Physics Reports* **1038**, 1 (2023).
 - [33] H. Tong, P. Tan, and N. Xu, From crystals to disordered crystals: A hidden order-disorder transition, *Scientific Reports* **5**, 15378 (2015).
 - [34] H. Ikeda, Jamming and replica symmetry breaking of weakly disordered crystals, *Phys. Rev. Res.* **2**, 033220 (2020).
 - [35] C. E. Maher, Y. Jiao, and S. Torquato, Hyperuniformity of maximally random jammed packings of hyperspheres across spatial dimensions, *Phys. Rev. E* **108**, 064602 (2023).
 - [36] P. Rissone, E. I. Corwin, and G. Parisi, Long-range anomalous decay of the correlation in jammed packings, *Phys. Rev. Lett.* **127**, 038001 (2021).
 - [37] E. Bitzek, P. Koskinen, F. Gähler, M. Moseler, and P. Gumbsch, Structural relaxation made simple, *Phys. Rev. Lett.* **97**, 170201 (2006).

- [38] T. S. Majmudar, M. Sperl, S. Luding, and R. P. Behringer, Jamming transition in granular systems, *Phys. Rev. Lett.* **98**, 058001 (2007).
- [39] H. Tong and H. Tanaka, Structural order as a genuine control parameter of dynamics in simple glass formers, *Nature Communications* **10**, 5596 (2019).
- [40] C. P. Goodrich, A. J. Liu, and S. R. Nagel, Finite-size scaling at the jamming transition, *Phys. Rev. Lett.* **109**, 095704 (2012).
- [41] D. Hexner, P. Urbani, and F. Zamponi, Can a large packing be assembled from smaller ones?, *Phys. Rev. Lett.* **123**, 068003 (2019).
- [42] C. E. Maher and S. Torquato, Hyperuniformity scaling of maximally random jammed packings of two-dimensional binary disks, *Phys. Rev. E* **110**, 064605 (2024).
- [43] J. Kim and S. Torquato, Methodology to construct large realizations of perfectly hyperuniform disordered packings, *Phys. Rev. E* **99**, 052141 (2019).
- [44] Y. Wang, Z. Qian, H. Tong, and H. Tanaka, Hyperuniform disordered solids with crystal-like stability, *Nature Communications* **16**, 1398 (2025).
- [45] D. Hexner, A. J. Liu, and S. R. Nagel, Two diverging length scales in the structure of jammed packings, *Phys. Rev. Lett.* **121**, 115501 (2018).